Dynamic Responses of a 1:5-Scale Ocean Current Energy Converter

S.-H. Yang, Y.-C. Hung, R.-Y. Yang, T.-E. Hou, L.-J. Mu, S.-W. Huang, J. Guo, and S.-M. Lin

Abstract—**The objective of this study is to numerically evaluate the dynamic responses of the Floating Kuroshio Turbine (FKT)—an ocean current energy converter—installed for field testing. In autumn 2022, the FKT was installed and tested at a 1:5 scale in the open sea area, located 1 kilometre off the LiuQiu Island coast, Taiwan. Because of unfavourable site conditions, the mooring and power cable systems for the FKT had to be customarily designed for the testing conditions. An investigation of the dynamic motions and structural responses of the mooring and cable systems was performed prior to physical testing to ensure the integrity of the testing campaign. The numerical analyses were performed using the commercial software DNV SIMA, where the prospect of the surfaced FKT and the mooring entanglement were evaluated and compared. This paper details the modelling process and the evaluation of the dynamics of the entire FKT system. Finally, the challenges and potential improvements for numerical assessments of a testing-oriented offshore marine energy system are identified and discussed.**

Keywords—**coupled dynamics, Dyneema mooring, marine current energy converter, mooring analysis, offshore energy converter, numerical simulation**

I. Introduction

The need to utilise clean renewable energy to reach the global mission of carbon neutrality has become prominent, now, more than ever. Among various sources of renewable energy is ocean current energy. The ocean current is defined as the movement of the water mass derived from wind-driven and thermohaline ocean circulation [1]. The power potential in ocean currents has been estimated to be approximately 5,000 GW [2]. Moreover, because ocean currents usually flow continuously in the same direction and have low variability [1], energy devices that harvest energy from ocean currents have been considered one type of technology with potential for development.

The development of ocean current energy converters (OCECs) has been driven mostly by Japan and the US. The water-column array of energy production units, which targets the Florida Current, was developed by Finkl and Charlier [3]. The developer OceanBased Perpetual Energy has developed three different OCECs, all targeting the Gulf Stream with varying operation depths. The same company recently announced a plan for the first ocean current energy farm [4]. Shirasawa *et al*. [5] developed an ocean current turbine to harness the energy from the Kuroshio ocean current; their device functions like an underwater kite that flows along the ocean current. Their towing experiments showed that the design exhibits good hydrostatic stability and achieves stable power generation. Kairyu, an ocean current turbine with a rated power of 100 kW, underwent a demonstration test in 2017 by IHI Corporation. Target power generation was achieved during the demonstration period, but instability around the turbine blade was observed owing to the variation in the current profile [6].

An OCEC named the Floating Kuroshio Turbine (FKT) has been under development by National Taiwan University in Taiwan since 2015. Extensive numerical analyses of the FKT have been performed using in-house numerical code and computational fluid dynamics [7-8]. A 1:25-scale model and a 1:5-scale prototypical model with a single rotor were built and tested through towing experiments in a towing tank and in the field in 2020 and 2021, respectively [9]. For further validation of the system performance, a testing campaign for the complete 1:5-scale

This work was supported by the National Academy of Marine Research Taiwan under the grant agreement No. NAMR111051.

S.-H. Yang, T.-E. Hou, L.-J. Mu, S.-W. Huang, and J. Guo are with the Department of Engineering Science and Ocean Engineering at the National Taiwan University, Taipei, Taiwan. (e-mail: hedyshyang@ntu.edu.tw, d07525002@ntu.edu.tw, d01525002@ntu.edu.tw, swhuang1983@ntu.edu.tw, jguo@ntu.edu.tw)

Y.-C. Hung was at the Department of Hydraulic and Ocean Engineering at the National Cheng Kung University, Tainan, Taiwan and is now at Sinotech Engineering Consultants Inc, Taipei, Taiwan. (e-mail: yuchi0402@mail.sinotech.com.tw)

R.-Y. Yang is with the Department of Hydraulic and Ocean Engineering at the National Cheng Kung University, Tainan, Taiwan. (e-mail: ryyang@mail.ncku.edu.tw)

S.-M. Lin is with the Department of Mechanical Engineering at the Kun Shan University, Tainan, Taiwan. (e-mail: smlin@mail.ksu.edu.tw).

Digital Object Identifier: https://doi.org/10.36688/ewtec-2023-150

model with two rotors was then proposed [10] and is the focus of this study.

This 1:5-scale test campaign was planned for a testing site approximately 1 km off the LiuQiu Island coast near Taiwan during the month of October 2022. According to the historical data of the test site, the maximum tidal current speed during the month of October is 1 m/s. Note that this current speed is significantly lower than the Kuroshio ocean current, with an average current speed between 1-1.5 m/s. The testing site, however, was chosen for its favourable depth and seabed conditions. The water depth is approximately 70 m. The seabed is mainly composed of clayey slit, where a gravity anchor can be applied.

Fig. 1 illustrates the overview of the field test. The FKT is moored to the seabed by a mooring system composed of Dyneema tethers, a steel chain, and a gravity anchor. Both the FKT and the mooring systems are the exact scaled model of the original design with only one exception; that is, the universal joint used in the mooring system is chosen to accommodate testing sites with varying tidal current directions.

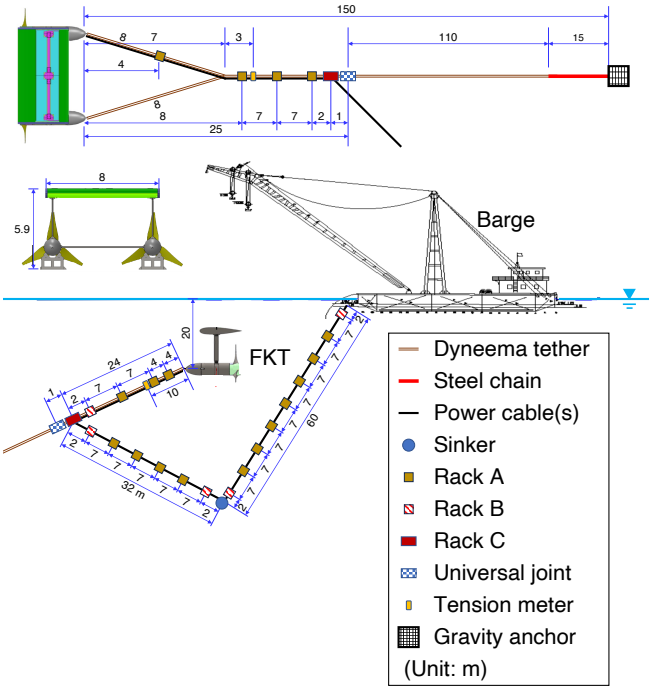

Fig. 1. Illustration of the setup of the field test (not to scale).

The design of the cable system is tailored to the testing conditions. Due to limited resources, it was decided prior to the test that a physical link must be made between the FKT and a floating barge. The barge was used to receive all the signals of measurement data or control the device under emergency conditions. Moreover, the cable system comprises three individual cables. Consequently, a relatively complex design of the cable system was made, where the entire system consists of three cables, multiple racks with different shapes, and a sinker. An understanding of the dynamic characteristics of the system setup was deemed necessary prior to physical testing to ensure the integrity of the testing campaign.

The objective of the current study is to evaluate the dynamic motion and structural responses of the entire FKT system with numerical methods. The critical concerns include the following:

1. Will the FKT be at risk of being grounded or surfaced due to the low current speed at the test site?
2. Does collision or entanglement occur between any components in the system?
3. Given that the testing period is during the typhoon season of the area, what is the expected maximum lifting force on the anchor?

Detailed designs of the testing setup and numerical model are presented in Section II. The results from the numerical simulations are presented and discussed in Section III. Discussions regarding the test campaign and the numerical investigation are presented in Section IV. Finally, a summary of the case study is concluded in Section V together with some suggestions for future work.

II. Design of the 1:5 FKT System for Field Testing

This section presents the experimental and numerical setup of the 1:5-scale FKT system; see Fig. 2 for an aerial photo of the test campaign.

Fig. 2. Aerial photo showing the FKT system near the LiuQiu Island coast.

A. *Floating Kuroshio Turbine*

The full-scale prototype design of the FKT was proposed with a rated power of 0.5 MW [10]. A schematic view of the 1:5-scale model of the FKT is illustrated in Fig. 3. The device is composed of a hydrofoil floating body, a buoyancy control system, two nacelles, two vertical supports, and a cross beam. Each turbine nacelle is equipped with a 10 kW power generator. Hence, the rated power of the 1:5-scale model is 20 kW. Fig. 4 presents the final production of the FKT device and its appearance when operating in water. Note that in the following discussion, all the data and results were reported for the exact 1:5-scale field test condition except as otherwise noted.

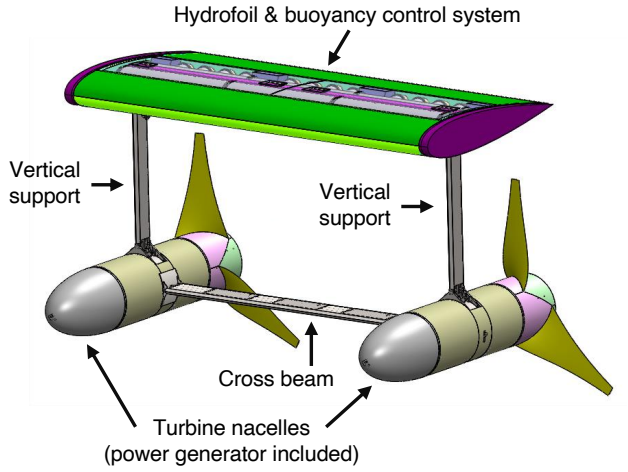

Fig. 3. Schematic view of the 20 kW FKT model.

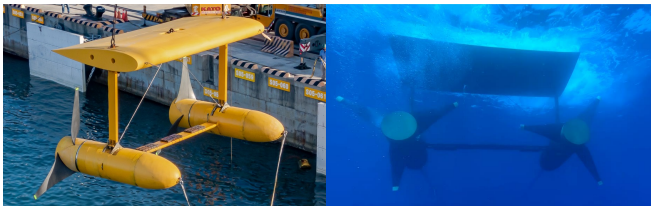

Fig. 4. (Left) Final production of the 1:5 FKT model and (right) the appearance of the FKT during operation.

In the numerical model, the origin of the reference Cartesian coordinate, (0, 0, 0 m), is placed in the plane of the water surface at the geometric centre of the FKT when the FKT freely floats in water. Note, however, that the initial position of the FKT device was defined at the coordinate of (0, 0, -20 m). The FKT device was assumed to be a rigid body that has six degrees of freedom (DoFs) of motion. The global response of the FKT device was evaluated by the hydrodynamic diffraction/radiation software WAMIT [11]. Table I presents the basic properties of FKT in the 1:5-scale model. The characteristic width, defined as the span of the hydrofoil, of the FKT is 8 m. On the other hand, the characteristic height of the FKT is 5.9 m, which is the distance between the top-most of the hydrofoil and the bottom-most of the turbine. For the numerical analysis, the viscous drag effect of the FKT device was represented by drag terms in three translational directions of motion. The quadratic drag coefficients, C_{dx}, C_{dy}, and C_{dz}, for the prediction of viscous drag were evaluated in [7] and used as the input in the current study.

TABLE I
BASIC PROPERTIES OF THE 1:5 MODEL OF FKT

Mass, M_{FKT} (kg)	19.234
Centre of gravity, CoG (m) [a]	-0.0448, 0.00225, -2.7939
Moment of inertia[a], I_{xx}, I_{yy}, I_{zz} (kgm^2)	3.3·10^5, 2.0·10^5, 1.5·10^5
Moment of inertia[a], I_{xy}, I_{yz}, I_{zx} (kgm^2)	162.96, -56.62, 2193.3
Drag coefficients, C_{dx}, C_{dy}, C_{dz} (-)	0.52, 0.71, 0.97
Initial position, (x, y, z) (m)	(0, 0, -20)

[a]The values are defined with respect to the reference point of the FKT itself. The FKT's reference point is placed at the geometric centre of the FKT at the plane of the water surface when the FKT freely floats in the water.

B. *Mooring system*

The mooring system consists of Dyneema tethers, a steel chain, and a gravity anchor. The steel chain is made of an R3 steel studless chain. The chain was used at the bottom of the mooring system and connects the anchor and the Dyneema tethers. The anchor was located at the coordinate of (0, 0, -70 m). In total, three segments of Dyneema tethers with various lengths were used. The first two shorter segments were used at the upper part of the mooring system, and they were connected to the FKT device, each on one nacelle. The coordinates of the two fairlead points are (0, 3.6, -23.9 m) and (0, -3.6, -23.9 m). The third longer Dyneema segment was used to connect the other two shorter Dyneema segments and the steel chain. Table II and Table III present the basic properties of the Dyneema tethers and the steel chain, respectively. In the numerical model, both Dyneema tethers and steel chains are represented by first-order bar elements with homogeneous cross-sectional properties. The bar element is constrained to exhibit stiffness in the axial direction only, and the corresponding structural responses are characterised solely by the axial force. The anchor is assumed to be a stationarily fixed point.

TABLE II
BASIC PROPERTIES OF THE DYNEEMA TETHER

Mass, M_{dy} (kg/m)	0.409
Nominal diameter, d_{dy} (m)	0.026
Axial stiffness, EA_{dy} (kN)	Represented by the load-strain diagram in Fig. 5
Length between the FKT and the 3-line joint, L_{dy1} (m)	7.89
Length between the 3-line joint and the connection point to the chain, L_{dy2} (m)	128.00
Breaking load, TBL_{dy} (kg)	59,600

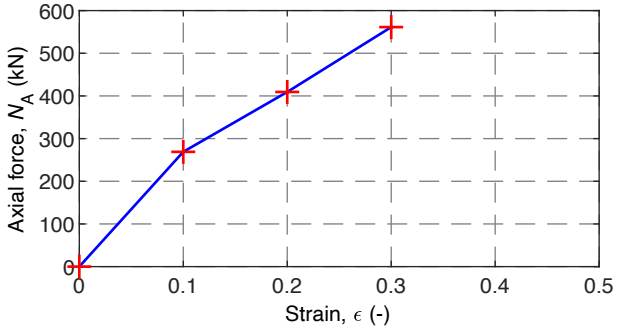

Fig. 5. Load-strain properties of the Dyneema tethers.

TABLE III
BASIC PROPERTIES OF THE STEEL CHAIN MOORING

Mass, M_{ch} (kg/m)	7.44
Nominal diameter, d_{ch} (m)	0.75
Axial stiffness, EA_{ch} (kN)	3.305·10^7
Length, L_{ch} (m)	15.00
Breaking load, TBL_{ch} (kg)	34,930

As illustrated in Fig. 1, parts of the mooring and power cable run on the same path and were bundled together by rack C; see Fig. 6 for the composition of different

components. Table IV presents the basic properties for various appendage components. In the numerical model, all the racks and sinkers (including those used in the cable system, see Section II.C) were all modelled as nodal points, which were defined exclusively by the mass, volume, added mass coefficients, and quadratic drag coefficients. It is assumed that all the mooring lines or power cables connect to the same nodal point in the numerical model if they are joined by the same rack or sinker. The rack or sinker follows the movements of the connected mooring or cable and has no motion DoF by itself.

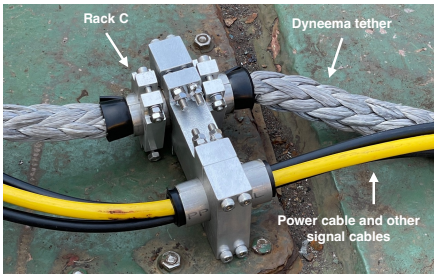

Fig. 6. The composition of the Dyneema mooring, power cable, and rack C.

TABLE IV
BASIC PROPERTIES OF APPENDAGE COMPONENTS

	Rack A	Rack B	Rack C	Sinker
Mass, M (kg)	3.5	4.8	3.5	100.0
Volume, V (m^3)	0.002	0.004	0.003	0.390

C. Cable system

Three cables were used in the field test for electricity and signal transmission. The three cables together with a sinker and the racks together constitute the cable system. The racks and the sinker were used together to ensure that (1) sufficient length of the cable is available for a buffer during the operation, (2) no excessive tension occurs anytime in the cable, and (3) no entanglement occurs between any components in the cable and mooring systems.

The link between the cable system and the FKT is located at one nacelle of the FKT, which was also the same fairlead point used for the mooring system. The other end of the cable system lies on the floating barge. Because the floating barge itself was not in the scope of the numerical study, the barge was assumed to be a stationary fixed point in the numerical model, and its coordinate was defined at (-16.8, 0, 0 m).

The detailed properties of the three individual cables were unavailable prior to the test. Hence, it was decided that the three cables were modelled as one equivalent cable in the numerical model. Table V presents the basic properties of the cable considered in the numerical model. The cable is modelled as the beam elements, and the mechanical properties of the cable account for stiffness in three directions. In the postprocessing of the numerical study, however, only the axial force in the cable was used for the results evaluation; these results were used as the reference value to search for appropriate cables for the field test.

TABLE V
BASIC PROPERTIES OF THE CABLE USED IN THE NUMERICAL STUDY

Mass, M_{ca} (kg/m)	0.405
Nominal diameter, d_{ca} (m)	0.015
Axial stiffness, EA_{ca} (N)	$2.2 \cdot 10^7$
Bending stiffness, EI_{ca} (Nm^2)	10.13
Torsion stiffness, GK_{ca} (Nm^2/rad)	$8.0 \cdot 10^4$
Length, L_{ca} (m)	92

D. Environmental conditions

The original concept of the FKT system was designed to target the Kuroshio ocean current with a target working environment at a water depth of approximately 500 m and a current speed of 1-1.5 m/s. Such an environment was, however, considered unrealistic for the 1:5-scale model testing stage. Hence, a test site with a shallower water depth and reasonable current speed was chosen instead.

The nearshore area of LiuQiu Island near Taiwan was chosen for the field test. The water depth of the test site is approximately 70 m. According to the historical measurement data, the maximum speed of the tidal current at the site was approximately 1 m/s at the water surface. However, because the direction of the tidal current varies, currents with different heading directions were considered in the numerical study. Finally, the testing period was selected because of the observed relatively high current speed of the year, which was unfortunately also within the typhoon season. As a result, the environmental conditions (ECs) considered in the numerical study covers both the normal monsoon sea state and the extreme typhoon sea state.

Table VI presents the 12 ECs simulated in the numerical study. Each EC was simulated by irregular loads that consist of waves and currents; the wind is not considered in the present study since its effect is deemed insignificant for the underwater operation of the FKT. The wave and current loads were assumed to align in the same incidence of direction, θ. The sea state was defined by the significant wave height, H_z, significant wave period, T_z, and spectral peak parameter, γ. The sea state follows the JONSWAP spectrum, and the γ-value was set to 3.3. The current speed at the water surface, V_{c0}, for each EC is defined in Table VI. The current load was assumed to be time-independent but depth-dependent following the current profile shown in Fig. 7. Hence, the current velocity magnitude at a specific water depth is defined as the product of V_{c0} and V_{cf} at the corresponding water depth. The duration of each environmental condition is set to 1 hr.

TABLE VI
DEFINITION OF THE ENVIRONMENTAL CONDITIONS FOR THE DETAILED STUDY BY THE NUMERICAL SIMULATION

Case ID	H_z (m)	T_z (s)	V_{c0} (m/s)	θ (°)
EC1	2.5	7.0	0.0	0
EC2	2.5	7.0	0.0	180
EC3	10.0	12.0	0.0	0
EC4	10.0	12.0	0.0	180
EC5	2.5	7.0	0.3	0
EC6	2.5	7.0	0.3	180
EC7	10.0	12.0	0.3	0
EC8	10.0	12.0	0.3	180
EC9	2.5	7.0	1.0	0
EC10	2.5	7.0	1.0	180
EC11	10.0	12.0	1.0	0
EC12	10.0	12.0	1.0	180

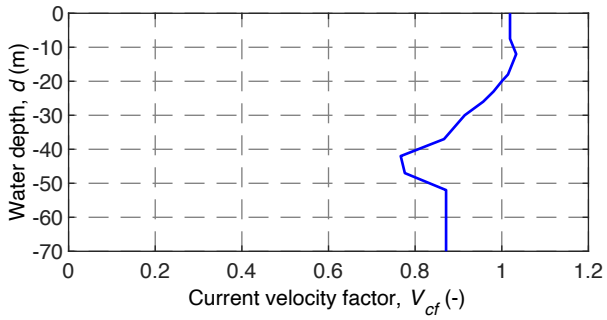

Fig. 7. Current speed profile in the depth direction.

E. *Simulation software*

The numerical analysis of the FKT systems was performed in DNV SIMA software [12]. SIMA comprises two solvers, namely, SIMO and RIFLEX. SIMO is responsible for the simulation of the FKT device, and it captures the motion of FKT in six DoFs. RIFLEX is used to solve the hydrodynamic forces on the mooring and cable systems and calculate their structural responses in terms of the motion and internal forces. The numerical simulation of the dynamic behaviour of the entire FKT system was performed by coupled response analysis in the time domain, as recommended in [13]. Fig. 8 presents the initial static configuration of the FKT system together with the Cartesian coordinate system.

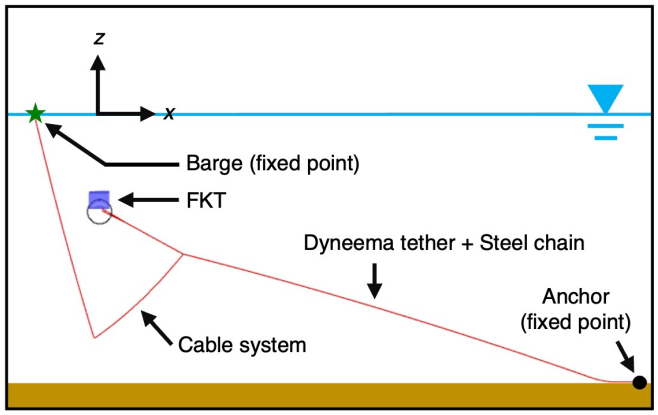

Fig. 8. Illustration of the static configuration of the FKT system in the numerical model.

III. RESULTS

The main focus of the numerical simulation was to evaluate the potential risk of the FKT being grounded or surfaced, as well as the collision or entanglement between any components in the system. The results from the numerical simulation are presented in this section, including the dynamic motion of the FKT device in Section III.A, and the structural responses of the mooring and cable systems in Section III.B.

A. *Dynamic motion of the FKT device*

Fig. 9 presents the horizontal trajectory of the FKT under case EC10; the corresponding vertical displacement of the device in the time domain is presented in Fig. 10. The case EC10 is deemed the test case that is likely to induce the most hazardous operation of the FKT system during the testing period. Fig. 9 shows that the minimal horizontal distance between the FKT device and the barge is approximately 10 m. In the vertical direction, the minimum clearance of the FKT either to the water surface or to the seabed was approximately 12 m.

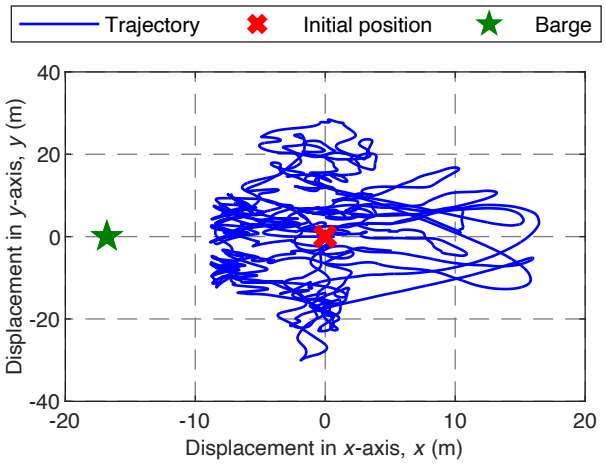

Fig. 9. Horizontal trajectory of the FKT under case EC10. The initial position of the FKT is represented by the red cross, and the fixed point of the barge is represented by the green star.

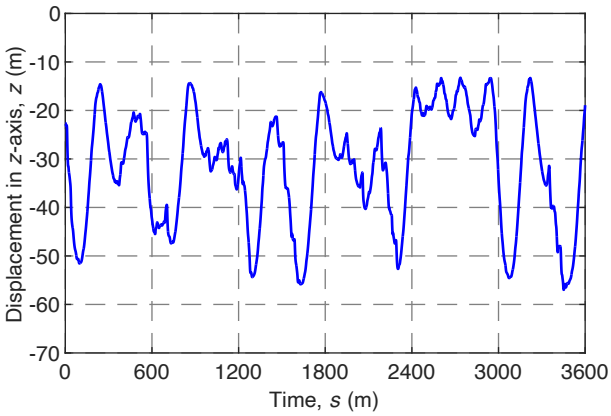

Fig. 10. Time history of the vertical displacement of the FKT under case EC10.

Figs. 11 to 13 present the overall range of displacement in the *x*-, *y*-, and *z*-axes for the FKT device under all simulated ECs. The results showed that when the current flow goes in the direction of 0° (i.e., all the odd-numbered cases), the range of the displacement in the *x*-axis is generally larger than that in the *y*-axis. On the other hand, the displacement in the *y*-axis was found to be more notable under the current direction of 180°, and this observation was even more pronounced when the current and wave coexist (namely, cases EC6, EC8, EC10, and EC12). Overall, the observed movement of the FKT in the *y*-axis is because the present design of the mooring system was more of a unidirectional mooring system and is less effective in constraining the transverse movement. Hence, although the current and wave were both acting in the main direction of the mooring system, significant movement of the FKT in the other direction was observed in most of the simulated cases.

The load direction of 0° always leads to a larger span of movement of the FKT than the load direction of 180°. A plausible explanation for the observation might be that the 0-degree load is more likely to cause the back-and-forth motions of the FKT, whereas the 180-degree load mainly causes the device to first move to the extreme position and only oscillate in a smaller area after.

Finally, a high likelihood of the FKT touching the seabed was observed under the typhoon sea state. Four out of six typhoon-related ECs, i.e., EC3, EC4, EC7, and EC12, show at least one incidence during the entire simulation where the displacement of the FKT in the *z*-axis falls below -69.9 m. In addition, a positive relation was found between the current speed and highest *z*-axis displacement of the FKT. The extreme case was found in cases EC9 and EC11, where the FKT was predicted to occasionally move out of the water surface. Overall, the results presented in this section reflect the fact that the present design for the field test was not intended to be used under typhoon conditions.

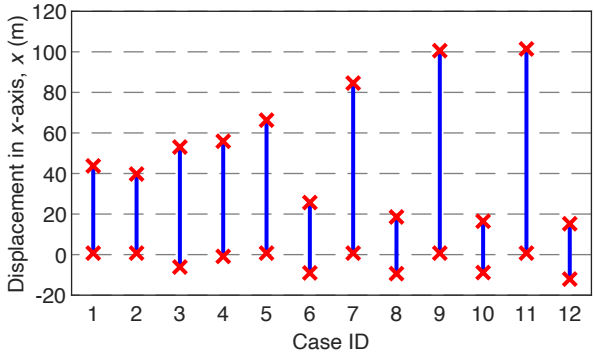

Fig. 11. Range of the displacement of the FKT device in the *x*-axis for all the tested ECs.

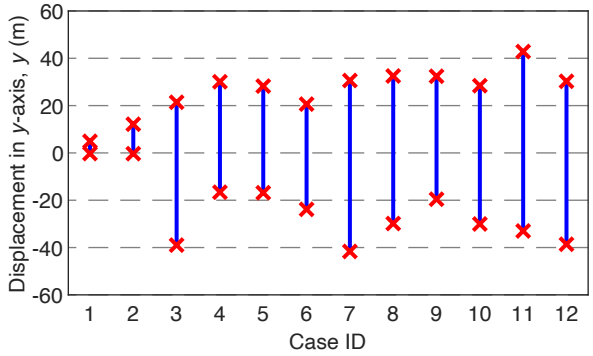

Fig. 12. Range of the displacement of the FKT device in the *y*-axis for all the tested ECs.

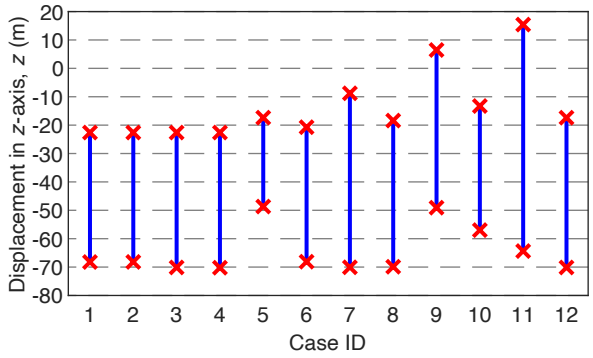

Fig. 13. Range of the displacement of the FKT device in the *z*-axis for all the tested ECs.

B. Structural responses of the mooring and cable systems

Fig. 14 and Fig. 15 present the force distribution along the mooring line and the cable under still-water conditions, respectively. The line coordinates of 0 m for the mooring and the cable are both defined at the fairlead point of each respective line. The other ends of the mooring and the cable are then defined at the anchor point on the seabed and at the floating barge, respectively. Abrupt changes in the axial force were found, and their positions correspond to the locations where the racks or sinker were installed.

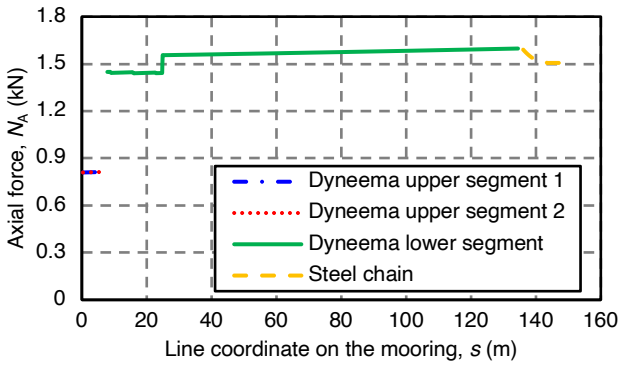

Fig. 14. Force distribution along the mooring lines under static conditions.

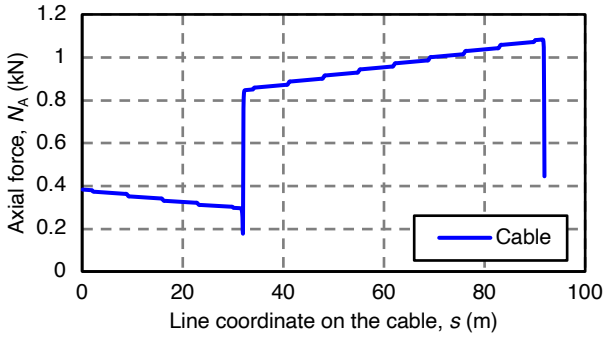

Fig. 15. Force distribution along the cable under static conditions.

Fig. 16 presents an example of the time domain results of the mooring and cable. The results were extracted from case EC10, and the force responses from the top end of each segment were plotted for comparison. A detailed investigation of the numerical results showed that the maximum force may not always occur at the top end of each segment owing to the presence of racks or sinkers. Hence, the maximum forces were examined along the entire mooring or cable; see the example results in Fig. 17 and Fig. 18.

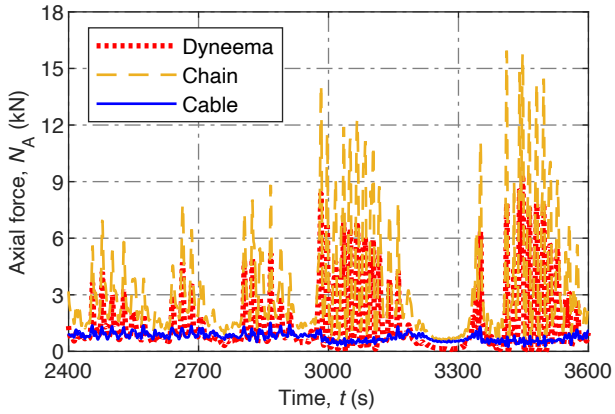

Fig. 16. Time domain responses at the top end of Dyneema, steel chain and power cable under case EC10.

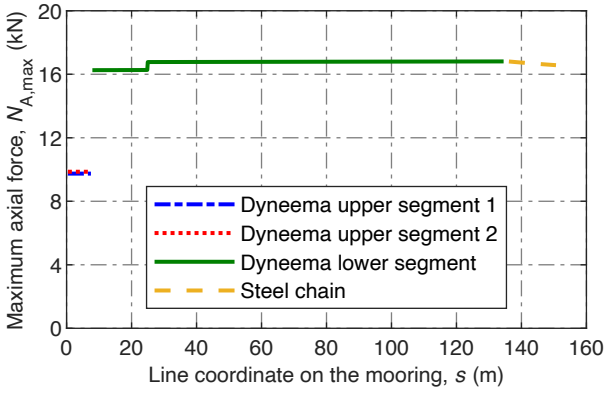

Fig. 17. Maximum axial force in the mooring for case EC10.

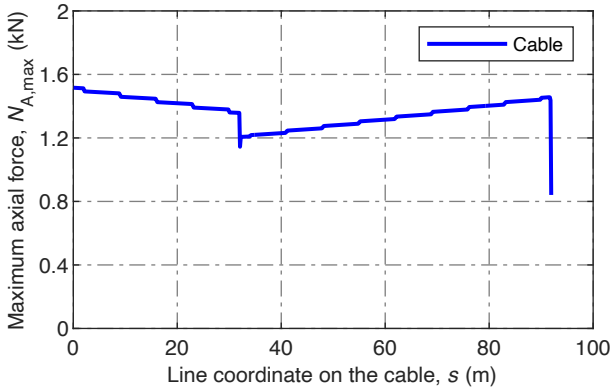

Fig. 18. Maximum axial force in the cable for case EC10.

To examine whether the extreme force responses in the mooring or cable exceed the limit, the maximum force found along the entire line was used as the final reference value for each EC. Fig. 19 presents the maximum calculated forces in different components for all the simulated cases. The extreme cases for the Dyneema tether and steel chain were both found in case EC10, whereas the maximum force of the cable was found in case EC11. Unfortunately, no clear relation can be drawn between the definition of the environmental conditions and the force responses in either mooring or cable. Nonetheless, the safety margin was deemed sufficient since the calculated maximum forces of the Dyneema tether and steel chain both represent only 20% of the minimum breaking load of the respective material.

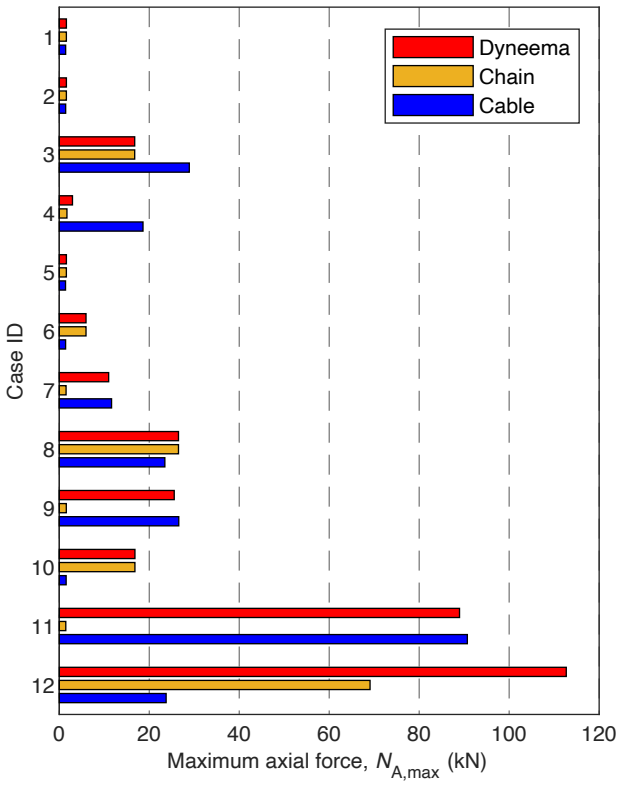

Fig. 19. Comparison of maximum forces in the Dyneema tether, steel chain, and cable.

Fig. 20 presents the prediction of the vertical force acting on the anchor, which was calculated by finding the *z*-component of the force in the mooring line element that connects to the seabed. Compared to the final design of the anchor, which has a maximum anchor force of 8.28 kN (shown as the red dash-dotted line in Fig. 20), the simulation results showed that the final design of the anchor was appropriate for the target operation environment.

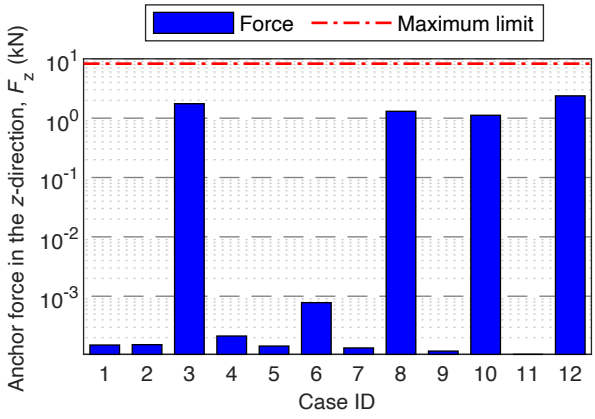

Fig. 20. Comparison of maximum vertical forces on the anchor. The red dash-dotted line shows the maximum limit of the anchor that was used in the field testing.

IV. Discussion

According to the simulation results, the force responses in the mooring and cable were both calculated to have a reasonable safety margin. The simulation also confirmed that the present experimental design was not intended to be used under typhoon conditions; the FKT device shows the risk of being surfaced or grounded under typhoon sea states during simulation.

An evaluation of the animated results of the simulation showed that the possibility of entanglement between different components in the system was low. The sinker was able to stabilise the movement of the cable and prevent contact between the cable system and mooring lines. However, owing to the low position of the FKT device under the typhoon sea state, as discussed in Section III.A, the presence of a sinker could also cause contact between the cable system and the seabed. Because the numerical model of the cable was a simplification of the original design, the contact issue of the cable system was not in the scope of this study. Further study could be conducted to evaluate the detailed dynamic motions of the cable system.

The field test of the FKT system was carried out between October 6-8 in 2022. During the testing period, an optic fibre was broken on the second day of the test, and hence, only limited mooring force measurement data were available. The ocean current speed during the testing period was found to be mostly below 0.5 m/s, and the tension force measurements were in the range between 0.98 and 4.41 kN. Compared to the maximum forces of the Dyneema tethers simulated in EC5 and EC6 being 1.57 kN and 5.90 kN, the simulation results were generally considered realistic, but detailed investigations are still required to verify the numerical model. Overall, most of the FKT system remained in good condition after the 3-day field test, which verified the overall design of the experimental system for the intended testing condition.

V. Conclusion

This study presents a numerical study of the 1:5-scale FKT system. The tested system consists of an FKT device, a mooring system, and a cable system. Because of the constraint from the site condition, the system was partly designed in a nonconventional way, i.e., using racks and floating barge. The details of the experimental setup and the numerical model are first presented in Section II. As shown by the numerical study, both Dyneema tethers and steel chains exhibit relatively low forces even under the typhoon sea state. The sinker in the cable system successfully prevents contact between any components in the system. However, some risks were observed in terms of the motion of the FKT device. The FKT device was found to likely touch the seabed or be exposed to the water surface, especially under typhoon conditions.

A workflow to combine various parts of the tested system in a numerical model is presented in the current study. Owing to the complexity of the original design of the field test, our study showed that some assumptions or simplifications in the numerical model would be necessary for a better understanding of the dynamic characteristics of the floating energy converter system. Enabling numerical simulations for novel ocean energy devices is of paramount importance to highlight the potential risks and provides timely evaluations against ever-changing design during the early concept-proving phases of ocean energy developments. For the operational critical metrics such as mooring tension forces, we observe general agreements between simulations and field test results.

The postprocessing of the measurement data is currently underway, and we plan to perform more detailed validation against the simulation results. The development of the numerical model of the FKT system will be continued to support system optimisation and the next-phase field test in concept development. Another challenge is acquiring suitable power cables for field tests of various marine energy devices. The adoption of existing cable designs or a novel cable development for the physical testing of marine energy devices would also be an important research direction for the marine energy sector to advance towards commercial realisation.

Acknowledgement

The authors gratefully acknowledge Yu-Ting Hung at National Taiwan University for her tireless support on the planning of the field test as well as the collection of the relevant information for the completion of the current study.

REFERENCES

[1] A. Lewis *et al.*, "Ocean energy," in "IPCC special report on renewable energy sources and climate change mitigation," Cambridge University Press, Cambridge, United Kingdom and New York, NY, USA, 2011. [Online] Available: http://srren.ipcc-wg3.de/report/IPCC_SRREN_Ch06.pdf

[2] World Energy Council, "World energy resources: marine energy 2016," 2016. [Online] Available: https://www.worldenergy.org/wp-content/uploads/2017/03/WEResources_Marine_2016.pdf

[3] C. W. Finkl and R. Charlier, "Electrical power generation from ocean currents in the Straits of Florida: Some environmental considerations," *Renewable and Sustainable Energy Reviews,* vol. 13, no. 9, pp. 2597-2604, 2009.

[4] OceanBased Perpetual Energy. "Homepage of OceanBased Perpetual Energy," 2023. [Online] Available: https://oceanbased.energy

[5] K. Shirasawa, K. Tokunaga, H. Iwashita, and T. Shintake, "Experimental verification of a floating ocean-current turbine with a single rotor for use in Kuroshio currents," *Renew. Energy,* vol. 91, pp. 189-195, 2016.

[6] T. Ueno, S. Nagaya, M. Shimizu, H. Saito, S. Murata, and N. Handa, "Development and demonstration test for floating type ocean current turbine system conducted in Kuroshio current," in *2018 OCEANS - MTS/IEEE Kobe Techno-Oceans (OTO)*, Kobe, Japan, 2018.

[7] F. C. Chiu, C. Y. Hsin, H. Y. Lin, and Y. H. Lin, "Development of a floating Kuroshio turbine equipped with a foil float: Deployment and recovery simulation," in *OCEANS' 2016 MTS/IEEE Shanghai*, Shanghai, China, 2016.

[8] T. E. Hou, L. J. Mu, S. W. Huang, E. Chen, F. C. Chiu, and J. Guo, "hydrodynamic parameter estimation of a 20kw floating Kuroshio turbine operating in steady state," in *2023 IEEE Underwater Technology (UT)*, Tokyo, Japan, 2023.

[9] J.-F. Tsai, Y.-X. Zeng, and F.-C. Chiu, "Study on the Hydrodynamic Performance of a Floating Kuroshio Current Turbine," in *Proceedings of the 3rd World Congress on Civil, Structural, and Environmental Engineering (CSEE'18)*, Budapest, Hungary, 2018.

[10] L. J. Mu, S. W. Huang, T. E. Hou, E. Chen, Y. T. Hung, F. C. Chiu, and J. Guo, "Development and sea trail of the floating Kuroshio turbine," in *2023 IEEE Underwater Technology (UT)*, Tokyo, Japan, 2023.

[11] WAMIT, Inc. WAMIT, V7 ed, Massachusetts, USA.

[12] DNV, 2022, SIMA, V4.4.0 ed, Det Norske Veritas (DNV), Høvik, Norway.

[13] S.-H. Yang, "Analysis of fatigue characteristics of mooring lines and power cables for floating wave energy converters," Ph.D. dissertation, Chalmers University of Technology, Gothenburg, 2018.